PNAS Nexus, 2024, 3, 1–12
https://doi.org/10.1093/pnasnexus/pgad446
Advance access publication 18 December 2023
Research Report

Conversion of raltegravir carrying a 1,3,4-oxadiazole ring to a hydrolysis product upon pH changes decreases its antiviral activity

Tomofumi Nakamura[a,b,*,1], Mayu Okumura[a,1], Nobutoki Takamune[c,1], Tatsunori Hirotsu[d], Masaharu Sugiura[e], Junichiro Yasunaga[a] and Hirotomo Nakata[a]

[a]Department of Hematology, Rheumatology, and Infectious Diseases, Graduate School of Medical Sciences, Faculty of Life Sciences, Kumamoto University, Honjyo 1-1-1, Chuo-ku, Kumamoto 860-8556, Japan
[b]Department of Laboratory Medicine, Kumamoto University Hospital, Honjyo 1-1-1, Chuo-ku, Kumamoto 860-8556, Japan
[c]Kumamoto Innovative Development Organization, Kumamoto University, Kurokami 2-39-1, Chuo-ku, Kumamoto 860-0862, Japan
[d]CyDing Company Limited, Oehonmachi 5-1, Chuo-ku, Kumamoto 862-0973, Japan
[e]Faculty of Pharmaceutical Sciences, Sojo University, Ikeda 4-22-1, Nishi-ku, Kumamoto 860-0082, Japan
*To whom correspondence should be addressed: Email: tomona@kumamoto-u.ac.jp
[1]T.N., M.O., and N.T. contributed equally to this work.
Edited By: Ian Wilson

Abstract

Raltegravir (RAL), a human immunodeficiency virus (HIV)-1 integrase inhibitor, has been administered as part of antiretroviral therapy. Studies in patients with HIV-1 have shown high variability in the pharmacokinetics of RAL, and in healthy volunteers, coadministration of proton-pump inhibitors has been shown to increase the plasma RAL concentrations. Here, we found that RAL containing a 1,3,4-oxadiazole ring is converted to a hydrolysis product (H-RAL) with a cleaved 1,3,4-oxadiazole ring at pH 1.0 and 13.0 conditions in vitro, thereby reducing the anti-HIV activity of the drug. The inclusion of cyclodextrins (beta-cyclodextrin [βCD], random methyl-βCD [RAM-βCD], and hydroxypropyl-βCD [HP-βCD]) can protect RAL from pH-induced changes. The conversion of RAL to H-RAL was detected by using various mass spectrometry analyses. The chromatogram of H-RAL increased in a time-dependent manner similar to another 1,3,4-oxadiazole-containing drug, zibotentan, using high-performance liquid chromatography. Oral bioavailability and target protein interactions of H-RAL were predicted to be lower than those of RAL. Moreover, H-RAL exhibited significantly reduced anti-HIV-1 activity, whereas combinations with βCD, RAM-βCD, and HP-βCD attenuated this effect in cell-based assays. These findings suggest that βCDs can potentially protect against the conversion of RAL to H-RAL under acidic conditions in the stomach, thereby preserving the anti-HIV-1 effect of RAL. Although clinical trials are needed for evaluation, we anticipate that protective devices such as βCDs may improve the pharmacokinetics of RAL, leading to better treatment outcomes, including reduced dosing, long-term anti-HIV-1 activity, and deeper HIV-1 suppression.

Keywords: raltegravir, HIV integrase inhibitor, oxadiazoles, beta-cyclodextrin

Significance Statement

Changes in the pH can readily lead to the conversion of drugs containing a 1,3,4-oxadiazole ring to hydrolysates, which may affect the biochemical activity of the drug. Cyclodextrins that protect raltegravir, an human immunodeficiency virus-1 integrase (HIV-IN) inhibitor, against such pH changes can help maintain its anti-HIV-1 activity, potentially leading to better treatment outcomes in patients with HIV.

Introduction

Raltegravir potassium (RAL; MK-0518, ISENTRESS) was approved in 2007 as the first-in-class of human immunodeficiency virus (HIV) integrase strand transfer inhibitors (INSTIs) for the treatment of HIV infection, which prevents the integration of HIV-1 DNA into the host genome (1). RAL has a well-established safety and efficacy profile in treatment-naïve and treatment-experienced patients (2, 3). Although RAL can be administered with or without meals, it is affected by food intake (4). The pharmacokinetics of RAL are not only characterized by higher patient variability (5) but are also affected by the coadministration of antacids (6) or proton-pump inhibitors (7), suggesting that the highly acidic conditions in the stomach may impact the pharmacokinetic parameters of the drug (8). In addition, in vitro studies have shown that

Competing Interest: The authors declare no competing interest.
Received: July 20, 2023. **Accepted:** November 14, 2023

divalent metals and pH changes alter RAL disposition (9), and impurities of RAL potassium drug substance have been observed during laboratory optimization (10). This study focused on pH changes and impurity C, a hydrolysis product, here termed H-RAL, in which the 1,3,4-oxadiazole ring is cleaved; the product is generated by water molecules with a hydrogen ion under acidic conditions or a hydroxide ion under alkaline conditions. We hypothesized that H-RAL may be generated in the acidic gastric solution. This conversion may affect the pharmacokinetics and anti-HIV-1 activity of orally administered RAL.

Cyclodextrins (CDs) are widely used in many fields, including the food, pharmaceutical, and cosmetic industries (11). Naturally occurring CDs, such as αCD, βCD, and γCD, are cyclic oligosaccharides consisting of six, seven, and eight D-glucose units, respectively, linked by α-1,4 glycosidic bonds to form a cyclic structure. CDs have a hydrophobic inner ring and hydrophilic outer ring, which allows encapsulation of various molecules, thereby protecting from light, ultraviolet light, heat, oxidation, hydrolysis, and unpleasant taste, as well as improving the solubility of insoluble substances (11–13). Naturally occurring CDs have been approved by the Food and Drug Administration (FDA) and the European Medicines Agency (EMA) as Generally Regarded As Safe (GRAS) for oral administration (14). The pharmaceutical applications of various CDs have been reviewed and reported by Loftsson and coworkers (12, 15–17). Modified CDs can also improve drug properties, such as solubility, stability, dissolution rate, and bioavailability (16–18), and control the immediate or delayed release of drugs during oral administration (19). We considered that CDs may protect against the generation of H-RAL from RAL, induced by pH changes, which could potentially affect the anti-HIV-1 activity and pharmacokinetics of RAL. Interestingly, some CDs have been shown to suppress HIV-1 replication at high concentrations (20, 21) and to reduce chronic inflammation caused by HIV-1 infection (22). Encapsulation of CDs with anti-HIV-1 drugs may not only improve the pharmacokinetics of the drug but also enhance its anti-HIV-1 activity. This advantage has the potential to improve treatment outcomes for patients with HIV.

Furthermore, the reuse of old and potent drugs such as RAL can be a cost-effective and beneficial treatment option for patients infected with HIV-1 in developing countries where access to newer and more expensive drugs may be limited.

Results

Structural changes in RAL, bictegravir, and darunavir in strongly acidic and alkaline conditions

We hypothesized that highly acidic conditions may induce structural changes in RAL. The chemical structures of RAL, bictegravir (BIC) (23), a second-generation INSTI, and darunavir (DRV) (24), an HIV-1 protease inhibitor, used in this study are shown in Fig. S1A. To examine the pH-dependent structural changes in RAL, we identified the post-treatment chromatograms of RAL in various pH buffers using reversed-phase high-performance liquid chromatography (HPLC). When RAL was treated with phosphate buffer at pH 7.0 for 7 days (D7), pre- and post-treatment peaks were detected in almost the same elution fraction (Fig. 1A); in contrast, treatment at pH 1.0 (HCl–KCl) for 24 h (D1) induced a severe peak decrease, and a new peak of a more hydrophilic substance appeared in the early-time fraction (Fig. 1A). This peak indicates that the structure of RAL was changed. BIC and DRV did not show any changes at pH 1.0 (Fig. S1B). Moreover, we confirmed the effect of a strongly alkaline condition (pH 13.0, sodium hydroxide [NaOH]–KCl) on RAL: new bimodal hydrophilic peaks appeared instead of the RAL peak (Fig. 1A). BIC was not affected by treatment at pH 13.0, while DRV was affected only at pH 13.0, as shown in Fig. S1B. Finally, we examined the effects of pH changes (pH 1.0, 2.0, 3.0, 5.5, 7.0, and 13.0) on RAL, and the percentages of drug concentration from the observed peaks are shown in Fig. S1D. These data suggest that strongly acidic (pH 1.0) and alkaline (pH 13.0) conditions can severely impact RAL structure compared with intermediate pH values (Fig. S1E).

Identification of the hydrolysis product of RAL using mass spectrometry

Of the various impurities of RAL potassium (A to I) identified during laboratory optimization (10), we focused on impurity C; as previously reported, this hydrolysis product of RAL (H-RAL) appears by stirring RAL with acetonitrile and aqueous KOH (Fig. 1B). To confirm the generation of H-RAL, we analyzed the structural changes in RAL at pH 1.0 on D1 and D7 (Fig. 1C and D) and at pH 13.0 on D1 (Fig. S1F–H) using LC-mass spectrometry (LC-MS), LC-tandem MS (LC-MS/MS), and high-resolution MS (HR-MS) (25). The RAL HPLC chromatogram was still detected on D1 at pH 1.0, while a new chromatogram was completely converted on D7 (Fig. 1A). This result was similar to that at pH 13.0 on D1 (Fig. 1A), suggesting that RAL converts to a different molecule in strongly acidic and alkaline conditions. Using LC-MS, an LC-MS spectrum of 463.17 mass/charge (m/z), corresponding to the theoretical m/z of H-RAL (463.174), was detected in the D1 and D7 samples at pH 1.0 (Fig. 1C) and in the D1 sample at pH 13.0 (Fig. S1F). Using LC-MS/MS analysis, fragmented spectra derived from 463.17 in the D1 and D7 samples at pH 1.0 and the D1 sample at pH 13.0 were also similarly detected (Figs. 1C and S1F), suggesting that the spectra at m/z 463.17 in the samples can be identified as the same molecule, H-RAL. The LC-MS chromatograms at pH 1.0 showed that ~50% of RAL was converted to H-RAL on D1 (Fig. S1I), whereas RAL had completely converted to H-RAL by D7; in contrast, no changes in the molecular weight (MW) of RAL treated with the pH 7.0 phosphate buffer on D1 were identified (Fig. S1J), consistent with the HPLC results. Moreover, we investigated the appearance of H-RAL using HR-MS, which is a high-precision quantitative analysis to identify the molecular formula of unknown substances. The measured m/z values of 463.1744 (D1) and 463.1747 (D7) clearly corresponded to the m/z 463.1736 of H-RAL, as assessed by err (−1.8 ppm for the D1 and −2.4 ppm for the D7 sample) that indicate mass accuracy, and mSigmas (5.3 for D1 and 6.3 for D7) that indicate isotopic pattern matching for fits between measured and theoretical values (Fig. 1D). These data demonstrate that conditions of pH 1.0 and 13 compel RAL to convert to H-RAL (Fig. S1H).

Hydrolysis of zibotentan containing a 1,3,4-oxadiazole ring

Various derivatives of commercially available drugs contain a 1,3,4-oxadiazole ring, including furamizole (an antibacterial drug), nesapidil (an antiarrhythmic drug), tiodazosin (an antihypertensive agent), zibotentan (an anticancer drug, ZD4054; Fig. 2A), and RAL (26) (Fig. S2A). Zibotentan is a specific, orally administered ET_A receptor antagonist in clinical development for the treatment of various types of cancer (27, 28). The chemical structures of ZD4054 and a putative hydrolysis product, H-ZD4054 are shown in Fig. 2A. We used HPLC to investigate the generation of these products after treatment at pH 1.0 and 7.0 for D1. ZD4054 chromatograms pre- and post-treatment at pH

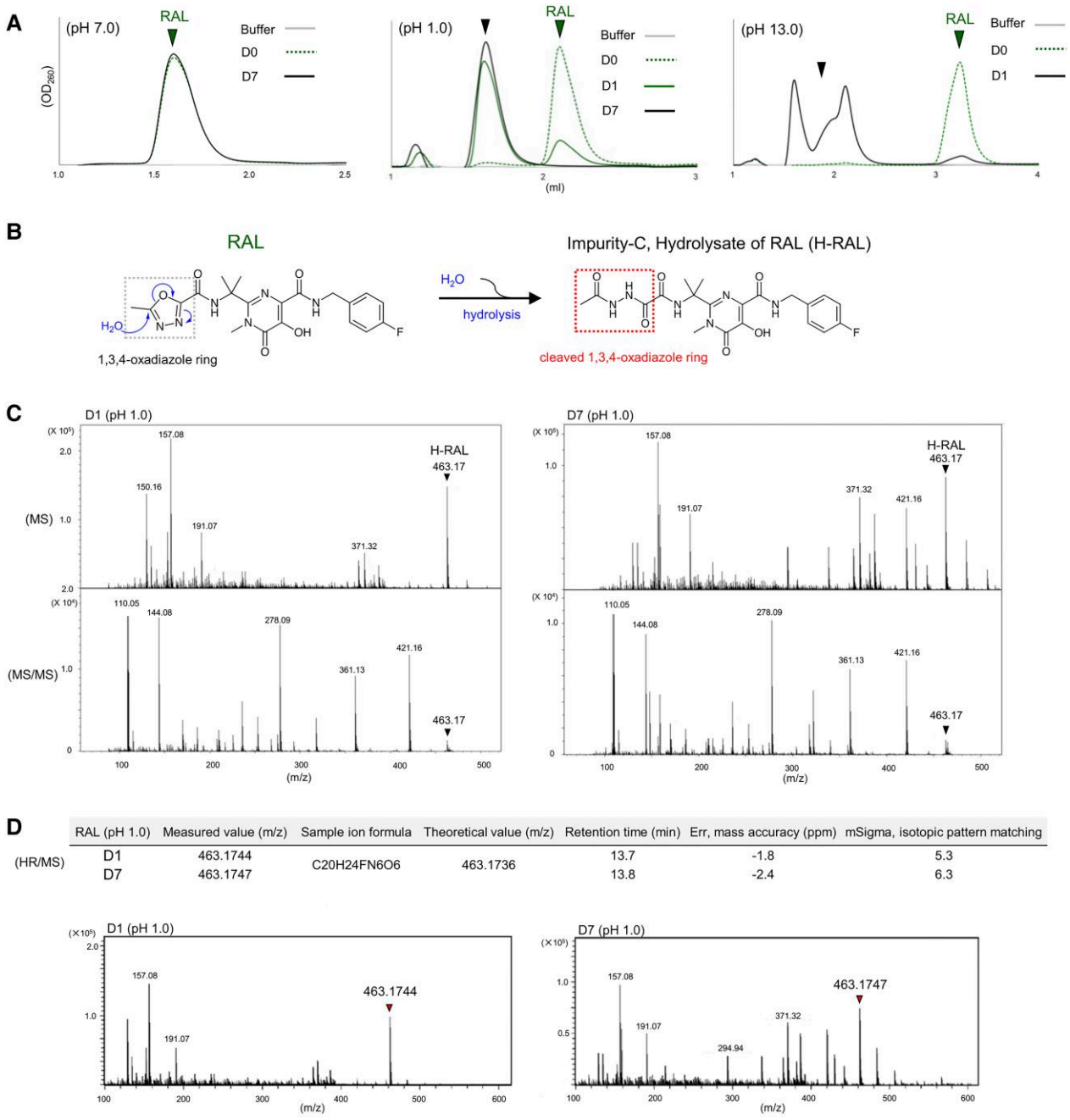

RAL (pH 1.0)	Measured value (m/z)	Sample ion formula	Theoretical value (m/z)	Retention time (min)	Err, mass accuracy (ppm)	mSigma, isotopic pattern matching
D1	463.1744	C20H24FN6O6	463.1736	13.7	-1.8	5.3
D7	463.1747			13.8	-2.4	6.3

Fig. 1. Structural changes of RAL induced by pH changes. A) The representative HPLC chromatograms of RAL are shown in green pre- and post-treatment at pH 7.0 on the left, pH 1.0 in the middle, and pH 13.0 on the right side for 24 h (D1) and/or D7, respectively. B) Putative chemical structure of RAL after hydrolysis reaction by pH changes. C) H-RAL spectra corresponding to *m/z* 463.17 of pH 1.0 post-treatment of RAL for D1 and D7 are detected by MS and MS/MS analysis. D) Measured H-RAL values for D1 and D7 at the retention times corresponding to the theoretical H-RAL values assessed by err and mSigma that indicate mass accuracy and isotopic pattern matching, respectively. The consistent spectra of *m/z* 463.1744 and 463.1743 for H-RAL after pH1.0 treatment for D1 and D7 were detected by HR/MS. The mSigma values indicating isotopic pattern matching below 20 are reliable for fits between measured and theoretical values. All assays were performed in two or three independent experiments and representative data are shown.

7.0 showed almost identical elution profiles (Fig. 2B). Conversely, at pH 1.0, the position of the ZD4054 chromatogram shifted to that of a more hydrophilic compound appearing in the early-time fraction (Figs. 2B and S2B). To confirm the structural changes of ZD4054 at pH 1.0, we performed HR-MS analysis. The chromatograms of ZD4054 at pH 1.0 on D1 showed conversion to H-ZD4054 at 70.1% (Fig. 2C). The measured *m/z* values of 425.1023 for ZD4054 (D0) and 443.1131 for H-ZD4054 (D1) correspond to the theoretical *m/z* values of 425.1027 for ZD4054 (D0) and 443.1132 for H-ZD4054 (D1) assessed by err (0.9 and 0.3 ppm) and mSigmas (15.0 and 11.9), respectively (Fig. 2D). Thus, after oral administration, drugs (RAL and ZD4054) containing the 1,3,4-oxadiazole ring can potentially be affected by the gastric environment.

Structure of CDs and inclusion models of RAL

CDs protect substances from hydrolytic reactions (12, 13). We examined whether CDs could inhibit RAL hydrolysis to H-RAL. Beta-CD, random methyl (RAM)-βCD, and hydroxypropyl

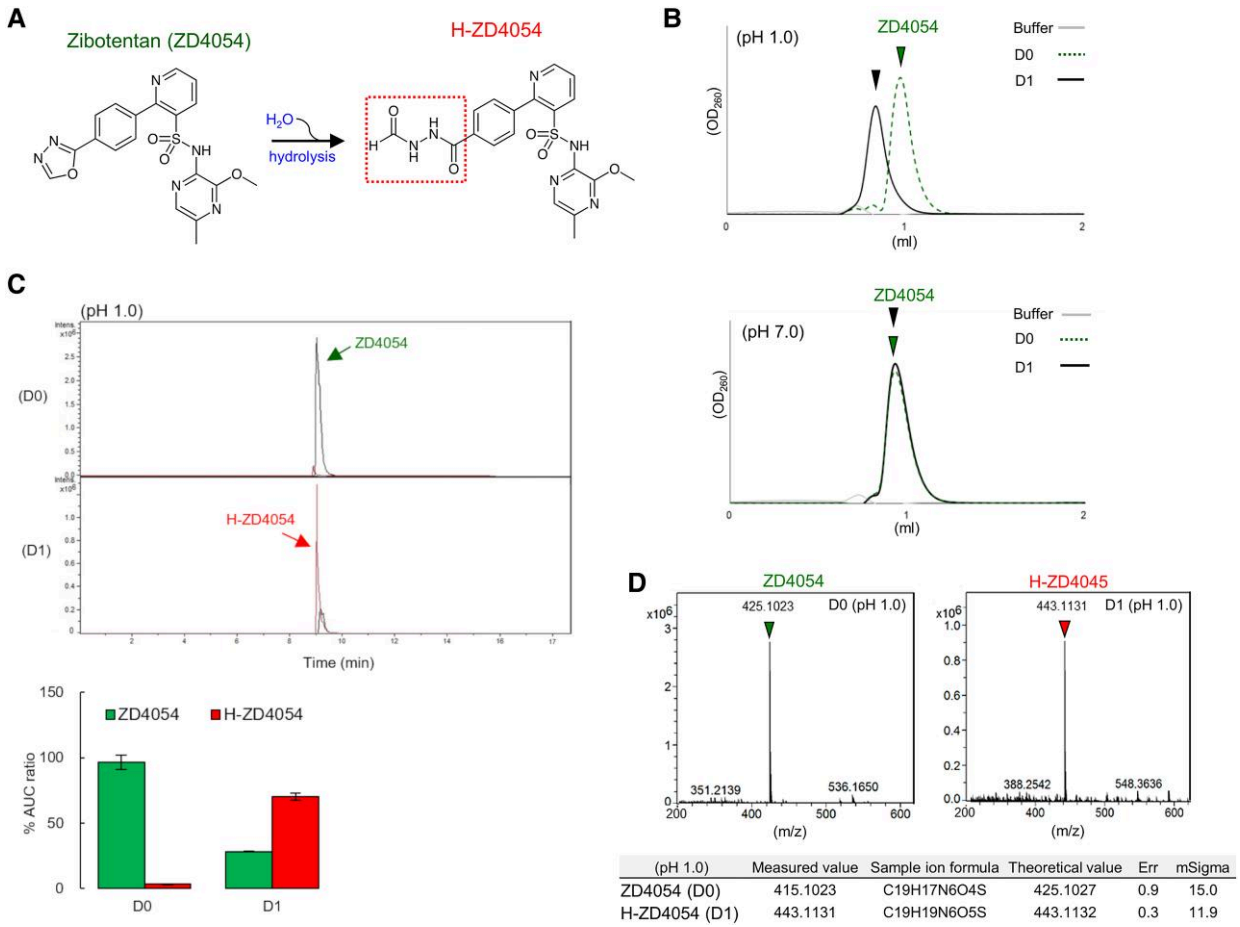

(pH 1.0)	Measured value	Sample ion formula	Theoretical value	Err	mSigma
ZD4054 (D0)	415.1023	C19H17N6O4S	425.1027	0.9	15.0
H-ZD4054 (D1)	443.1131	C19H19N6O5S	443.1132	0.3	11.9

Fig. 2. The structural changes of zibotentan post-treatment at pH 1.0. A) Chemical structure of zibotentan (ZD4054) containing a 1,3,4-oxadiazole ring and a putative hydrolysis product, H-ZD4054 which cleaved the 1,3,4-oxadiazole ring. B) The structural changes of ZD4054 to H-ZD4054 at pH 1.0 and pH 7.0 for D1 at 37 °C using HPLC. C) The chromatograms and % area under the curve, AUC ratio of the chromatograms at D0 and D1 of ZD4054 shown in green and H-ZD4054 in red are shown from D0 to D1 at pH 1.0 at 37 °C using LC-HR/MS. D) The measured *m*/*z* values correspond to the theoretical *m*/*z* values of ZD4054 and H-ZD4054 evaluated by err and mSigma in the table. The representative chromatograms of ZD4054 indicated by the arrow for D0 and H-ZD4054 indicated by the arrow after pH 1.0 treatment for D1 are detected by HR/MS. Representative data are shown and error bars indicate ± SD from two independent experiments.

(HP)-βCD (12, 15, 18) were used in this study (Fig. 3A). RAM-βCD and HP-βCD models containing seven methyl and hydroxypropyl groups, respectively, were generated from βCD (PDB accession number 3CGT [29]) using SeeSAR. Next, we investigated whether RAL could be included in these βCDs using docking simulation, surface plasmon resonance (SPR), and electrospray ionization mass spectrometry (ESI-MS) (30). Representative binding models of RAL to βCD, RAM-βCD, and HP-βCD generated by SeeSAR are shown in Fig. 3A. SPR was performed to assess the interaction of RAL, BIC, and DRV with multi-NH_2-βCDs immobilized on a sensor chip using Biacore X100. DRV was hardly binding to multi-NH_2-βCDs (Fig. S3A), while RAL interacted strongly with multi-NH_2-βCDs compared to BIC (Fig. 3B). The ESI-MS *m*/*z* spectra of the tested drugs and various CDs corresponding to the theoretical MWs are shown in Fig. 3C. The *m*/*z* spectra of BIC included in RAM-βCD or HP-βCD corresponding to the theoretical MWs (BIC plus RAM-βCD or BIC plus HP-βCD) were not detected. In contrast, those of RAL included into βCD, RAM-βCD, or HP-βCD corresponded to the theoretical MWs; the results were similar to those using SPR (Fig. 3B). These data indicate that RAL can be encapsulated into βCD, RAM-βCD, and HP-βCD; this process may provide RAL with the advantages of CDs, such as protection and stabilization under various conditions.

Impact of pH changes on RAL in the presence or absence of CDs

We hypothesized that RAL might be hydrolyzed and converted to H-RAL under highly acidic conditions in the stomach. The structural changes of RAL were analyzed over time after treatments in buffers at pH 1.0 or pH 13.0. At pH 1.0, the HPLC chromatograms of RAL at 2.1 mL fraction decreased in a time-dependent manner by ~25% at 3 h, 40% at 6 h, and 50% at 12 h and were completely converted to the H-RAL chromatogram around the 1.6 mL fraction at 72 h (D3) (Fig. 4A). Likewise, at pH 13.0, the HPLC peaks of RAL (3.2 mL fraction) decreased by 50% at 6 h, and new bimodal peaks appeared in the 1.5–2.5 mL fractions at 24 h (D1) (Fig. S4A). H-RAL was generated from RAL earlier at pH 13.0 than at pH 1.0. The structure of RAL was susceptible to pH changes, such as strongly acidic and alkaline conditions, over several hours, suggesting that, after oral administration, RAL could potentially be converted to H-RAL within hours in the strongly acidic conditions of the stomach. CDs may protect substances that are susceptible to hydrolysis from such pH changes (12, 13). Therefore, we examined whether βCD, RAM-βCD, and HP-βCD could protect against RAL conversion when treated at pH 1.0 for 0, 1, 3, and 6 h. Interestingly, mixtures of RAL with βCD, RAM-βCD, or HP-βCD significantly attenuated the decrease

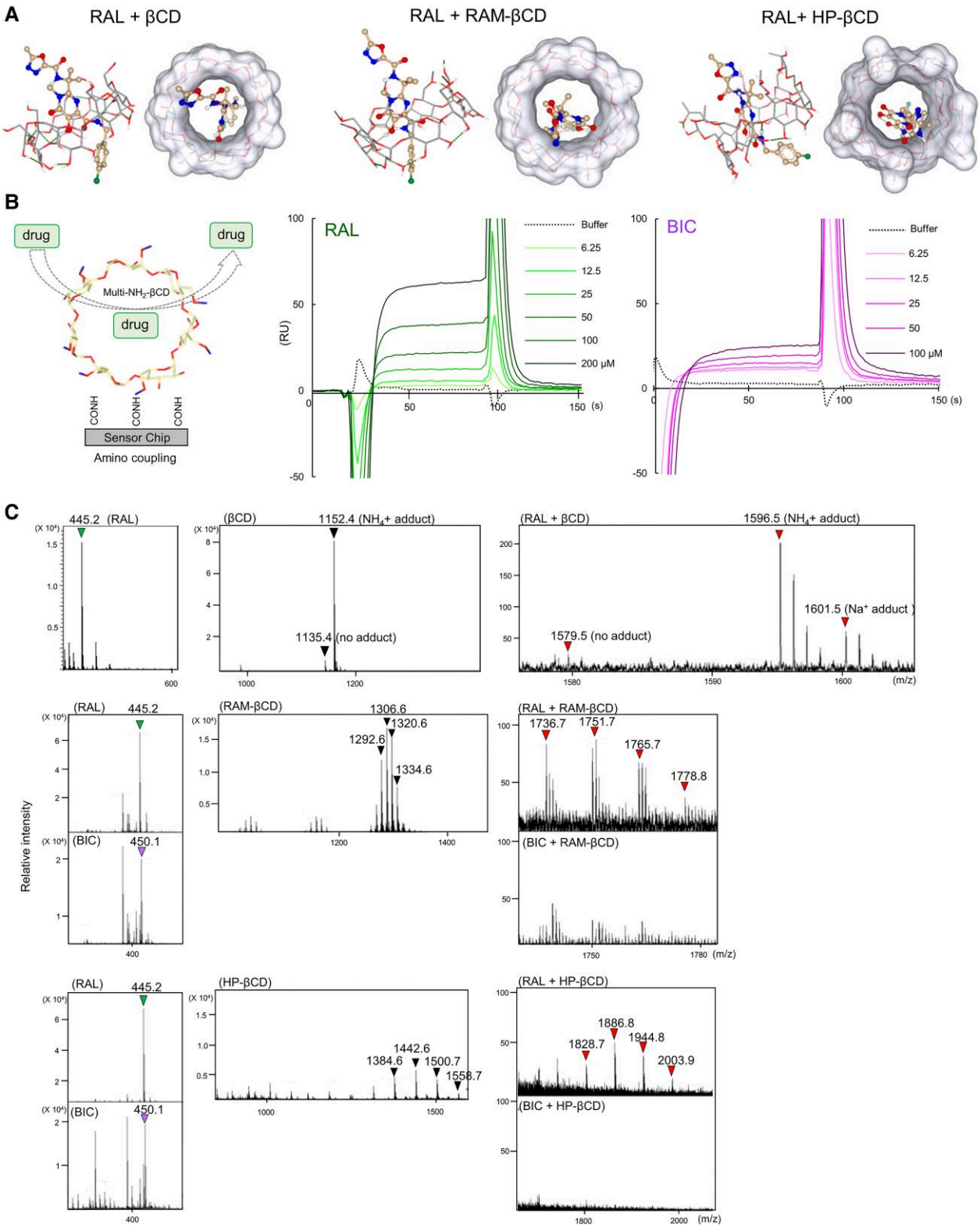

Fig. 3. Inclusion of RAL into CDs. A) The structure of βCD is used from the crystallography (PDB ID 3GCT). Those of RAM-βCD and HP-βCD are produced by the addition of side chains, 6-methyl and 6-hydroxypropyl groups, respectively, to the βCD, and representative binding models of RAL to βCD, RAM-βCD, and HP-βCD are generated by SeeSAR. Nitrogen, oxygen, carbon, and fluorine atoms of the molecules are shown in blue, red, pale orange, and green colors, respectively. B) SPR illustrated the interaction of the drugs with multi-NH_2-βCDs immobilized on a sensor chip. Sensorgrams of each concentration of RAL on the middle and BIC on the right side interacting with multi-NH_2-βCDs are detected. C) The representative *m/z* spectra of RAL shown by the green arrow, BIC by the purple arrow, RAL plus βCD, RAL plus RAM-βCD, and RAL plus HP-βCD by the red arrows, are detected by ESI-MS. The spectra of RAL plus βCD are mostly found by adding Na+ or NH_4+ to RAL plus βCD. The different *m/z* spectra of RAL plus RAM-βCD and RAL plus HP-βCD are shown because each RAM-βCD and HP-βCD contains a different number of side chains.

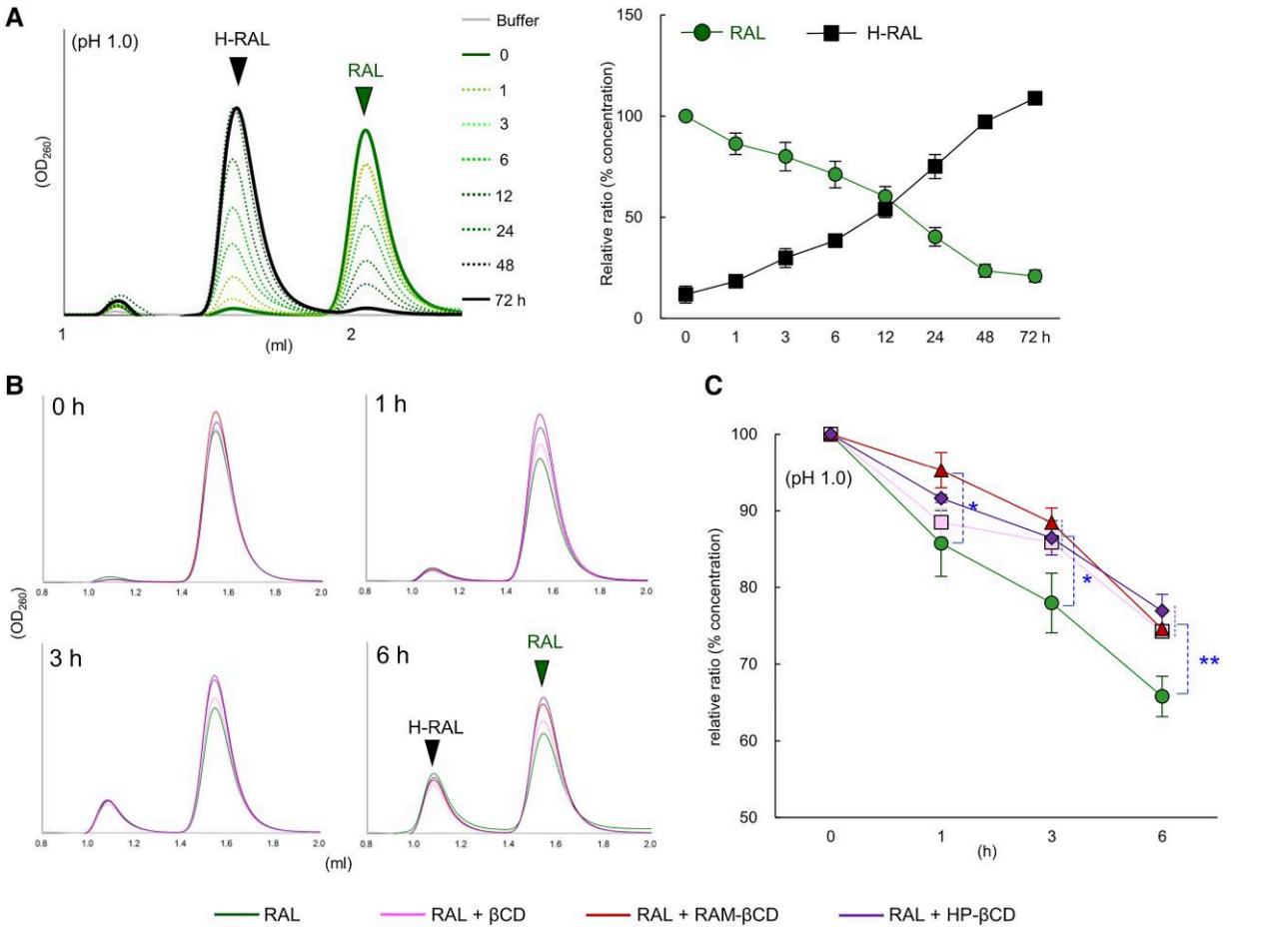

Fig. 4. Time-dependent changes of RAL to H-RAL and protection of CDs upon pH 1.0 treatment. A) The representative HPLC chromatograms on the left side and the % concentration on the right side of RAL and H-RAL are shown in a time-dependent manner from 0 to 72 h at pH 1.0 treatment. B) The conversion of RAL to H-RAL was detected when RAL, RAL plus βCD, RAL plus RAM-βCD, and RAL plus HP-βCD were incubated at 37°C for 0, 1, 3, and 6 h using HPLC. C) The line graphs indicate the % concentration of RAL alone and RAL mixed with βCD, RAM-βCD, and HP-βCD incubated at 37°C for 0, 1, 3, and 6 h, respectively. Error bars indicate ± SD from three independent experiments. Statistical significance was determined by Student's t test (*$P < 0.05$, **$P < 0.005$).

in the RAL peak (Fig. 4B and C) and suppressed the appearance of H-RAL (Fig. S4B) at pH 1.0 for 3 and 6 h compared to RAL alone. These results suggest that under highly acidic conditions (pH 1.0), such as those in the stomach, βCD, RAM-βCD, and HP-βCD can potentially protect RAL from conversion to H-RAL over time after oral administration.

H-RAL-binding models to prototype foamy virus integrase

The chemical structure of H-RAL contains a cleaved 1,3,4-oxadiazole ring induced by hydrolysis. The MW, LogP (partition coefficient), CLogP (calculated partition coefficient), LogS (aqueous solubility), and TPSA (topological polar surface area) scores that predict the pharmacokinetic properties (31) of RAL and H-RAL are shown in Table S1. These scores indicate that the fat solubility and cell membrane penetration of H-RAL are lower than those of RAL, which may lead to poor oral bioavailability of the drug. We examined whether the structural change in RAL affected its interaction with the target protein of HIV-IN. To analyze the interaction of H-RAL with HIV-IN, we performed a docking simulation using crystallography (PDB accession numbers 3L2V, 3OYA, and 7OUG) (32–34). These structures allowed us to use RAL-binding cavities consisting of the prototype foamy virus (PFV) or Simian T-lymphotropic virus 1 (STLV-1) IN protein, viral DNA, and catalytic metal cations. INSTI-binding models can substitute the HIV intasome for the PFV or STLV-1 intasome (34, 35), and H-RAL-binding models were generated based on the templates in which RAL binds to the PFV or STLV-1 intasome. As previously reported (32–34), the interaction of RAL with the binding cavity of the IN intasome dislocates the terminal 3′ nucleotide of the viral DNA and appears to inhibit metal cation (Mn^{2+} or Mg^{2+})-dependent activities (Figs. 5A, B and S5). The 4-fluorobenzene ring of RAL embedded within the binding pocket formed in place of the 3′ adenosine of the viral DNA, and the 1,3,4-oxadiazole ring fit into hydrophobic cavities including Tyr 212 or Tyr 149. These RAL rings interact with the side chains of Pro 214 or Pro 151 and Tyr 212 or Tyr 149, corresponding to HIV-IN Pro 145 and Tyr 143, respectively, forming hydrophobic and stacking interactions (Π–Π interactions) (Figs. 5B and S5) (36). The best H-RAL-binding structures, based on the RAL-binding templates of 3L2V, 3OYA, or 7OUG were selected from the top 10 models that were produced by SeeSAR (Figs. 5C and S5). The cleaved 1,3,4-oxadiazole ring in these binding models of H-RAL lost the capacity for Π–Π interactions with the side chain of Tyr 212 (Figs. 5C and S5). These data suggest that the interaction of H-RAL with the INSTI-binding cavity in the HIV-1 intasome may be weaker than that of RAL.

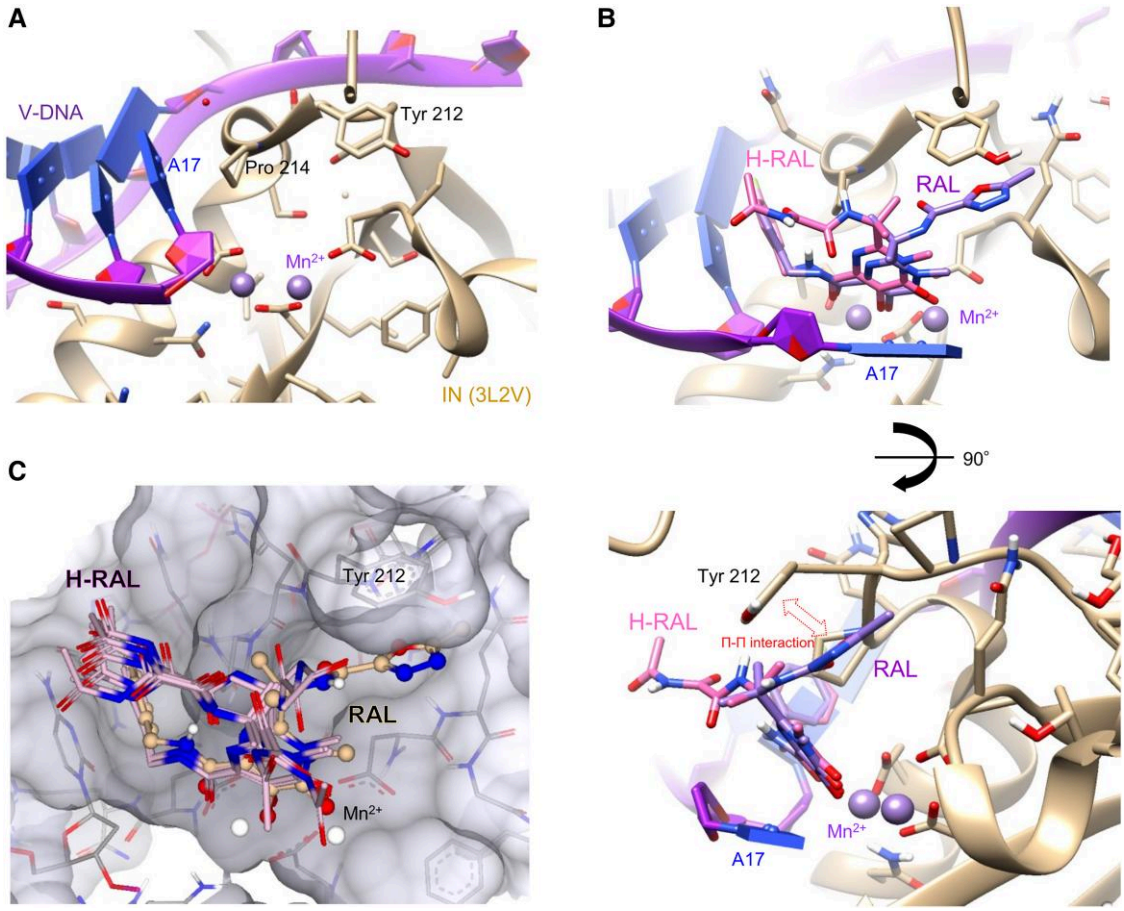

Fig. 5. Estimated binding models of H-RAL to PFV intasome. A) INSTI-binding pocket shown in PFV intasome containing PFV integrase, viral DNA (3′ adenosine, A17), and divalent cations Mn^{2+} (PDB ID, 3L2V). B) A best-fit model of H-RAL superimposed with RAL binding to the binding pocket of PFV-IN intasome. The 1,3,4-oxadiazole ring of RAL, but not H-RAL, fits into a hydrophobic cavity including Tyr 212 via a **Π–Π** interaction. C) Top 10 binding models of H-RAL interacting with the binding pocket generated by the docking simulation from the RAL-binding template of 3L2V. The carbons of PFV, RAL, H-RAL, and Mn^{2+} are shown in tan, purple, hot pink, and plum colors, respectively. The viral DNA structure is shown in magenta and blue. Nitrogen, oxygen, carbon, and fluorine atoms of the molecules are shown in blue, red, pale orange, and green colors, respectively. Molecular graphics were created using UCSF Chimera. All docking simulations were performed with SeeSAR v12.1.

Table 1. Anti-HIV-1 infectivity of RAL and BIC treated at pH 1.0, 7.0, and 13.0 for D0, D1, and D7 against HIV-$1_{VSVG\text{-}NL4\text{-}3}$ using TZM-bl assay.

TZM-bl assay		EC_{50} (nM)		
Drugs	**Day**	**pH 1.0**	**pH 7.0**	**pH 13.0**
RAL	D0	12 ± 2 (1)	6.8 ± 1.5 (1)	13 ± 0.01 (1)
	1	43 ± 7 (3.6)	6.5 ± 1.7 (0.9)	50 < (3.9<)
	7	1,000 < (83.3<)	7.6 ± 1.7 (1.1)	1,000 < (76.9<)
BIC	D0	4.1 ± 0.5 (1)	3.3 ± 0.5 (1)	3.7 ± 0.7 (1)
	1	4.3 ± 1.4 (1.0)	3.1 ± 0.3 (0.9)	3.9 ± 0.8 (1.1)
	7	4.8 ± 1.4 (1.0)	5.7 ± 1.6 (1.7)	4.5 ± 1.6 (1.4)

TZM-bl cells (5×10^4/mL) were exposed to diethylaminoethyl-dextran (25 μg/mL) plus HIV-$1_{VSVG\text{-}NL4\text{-}3}$ (50 ng/mL of p24) for 48 h in the presence of post-treatment with drugs at each concentration. Lysed cells were reacted with D-luciferin. EC_{50}s were determined from the luciferase intensity of the samples measured with FluoSTAR Omega. All assays were performed in duplicate, and the data shown are the mean values (±SD) of three independent experiments.

Table 2. Anti-HIV-1 replicative capacity of RAL, BIC, and DRV treated at pH 1.0, 7.0, and 13.0 for D0, D1, and D7 using MTT assay.

MTT assay		EC_{50} (nM)		
Drugs	**Day**	**pH 1.0**	**pH 7.0**	**pH 13.0**
RAL	D0	9.6 ± 3.2 (1)	5.4 ± 0.8 (1)	10.2 ± 7.5 (1)
	1	34 ± 1.7 (3.5)	8.0 ± 0.3 (1.5)	102 ± 58.0 (10)
	7	500 < (52.1<)	17 ± 6.3 (3.2)	500 < (49.0<)
BIC	D0	1.8 ± 1.0 (1)	2.4 ± 0.4 (1)	1.7 ± 0.1 (1)
	1	1.9 ± 0.2 (1.1)	2.2 ± 0.2 (1)	2.6 ± 1.0 (1.5)
	7	1.0 ± 0.1 (0.55)	1.8 ± 0.9 (0.8)	2.1 ± 0.1 (1.2)
DRV	D0	3.8 ± 2.2 (1)	5.6 ± 0.8 (1)	10.3 ± 0.2 (1)
	1	5.2 ± 2.8 (1.0)	3.0 ± 0.2 (0.5)	1,000 < (97.1<)
	7	3.2 ± (0.8)	4.9 ± 2.7 (0.9)	—

MT-2 cells (2×10^4/mL) were exposed to 100 $TCID_{50}$ of HIV-1_{LAI} and cultured in the presence of various concentrations of each drug post-treatment, and the EC_{50} values (50% effective concentration) and fold changes after each pH treatment for D0, D1, and D7 were determined by MTT assay. (Fold change; over 3-fold is shown in red.) All assays were performed in duplicate, and the data shown are the mean values (±SD) of three independent experiments.

Anti-HIV-1 activity of drugs and protection of RAL by CDs at pH 1.0

MT-2 cell viability of drugs (RAL, BIC, or DRV) and CDs (βCD, RAM-βCD, or HP-βCD) was examined using 3-(4,5-dimethylthiazol-2-yl)-2,5-diphenyltetrazolium bromide (MTT) assay (37) (Table S2). The anti-HIV-1 infectivity of RAL and BIC at pH 1.0, 7.0, and 13.0 on D0, D1, and D7 were evaluated using TZM-bl assay with VSV-G pseudotyped HIV-$1_{NL4\text{–}3}$ (HIV-$1_{VSV\text{-}G\ dENV}$) (Table 1 and Fig. S6A), and the anti-HIV-1 reproductive capacity of RAL, BIC, and DRV were assessed using MTT assay with HIV-1_{LAI} (Table 2 and Fig. S6B) (38). The anti-HIV-1 activity (50% effective concentration [EC_{50}]) of RAL at

pH 7.0 on D1 (EC_{50} 6.5 nM) and D7 (EC_{50} 7.6 nM) was similar to that on D0 (EC_{50} 6.8 nM) based on the results of the TZM-bl assay (Fig. S6C and Table 1). In contrast, the anti-HIV-1 activity of RAL at pH 1.0 on D1 decreased by 3.6-fold (EC_{50} 43 nM) compared to that on D0 (EC_{50} 12 nM). On D7, RAL (consisting mainly of H-RAL) activity further decreased by 83.3-fold to EC_{50} > 1,000 nM (Fig. 6A and Table 1). The anti-HIV-1 activity of RAL at pH 13.0 on D1 and D7 decreased to EC_{50} > 50 nM and >1,000 nM, respectively (Fig. 6B and Table 1). The second-generation INSTI, BIC did not show a decrease in anti-HIV-1 activity at pH 1.0 and 13.0 (Fig. S6D and E, Table 1). Similarly, MTT assay was performed to observe the inhibition of HIV-1 replication induced by RAL, BIC, and DRV post-treatment at pH 1.0 and 13.0 (Table 2). The EC_{50} values of RAL and BIC were consistent with those obtained using TZM-bl assay described above (Table 1). Next, the capacity of βCD, RAM-βCD, and HP-βCD for the protection of RAL from hydrolysis was evaluated using TZM-bl assay (Fig. S6A and F). Treatment with RAL at pH 1.0 without CDs resulted in gradually decreased EC_{50} values at 0, 3, and 6 h (EC_{50} values: 6.5, 12, and 17 nM, respectively; Figs. 6C and S6G). On the other hand, preparations of RAL and CDs at a molar ratio of 1:5 significantly attenuated the time-dependent decrease in these EC_{50} values, except for HP-βCD at 6 h (Figs. 6C and S6G). These results suggest that these CDs have sufficient potential for protection of RAL against hydrolysis to H-RAL.

Taken together, our findings demonstrate that RAL is readily converted to the hydrolysis product H-RAL under extreme pH conditions (pH 1.0 and 13.0) and that this conversion results in decreased anti-HIV-1 activity. This reduction can be alleviated in vitro by the formation of inclusion complexes with CDs such as βCD, RAM-βCD, and HP-βCD (Fig. 6D).

Discussion

RAL has made a significant contribution to the treatment of HIV infection. Discontinuation of RAL is rare because it is well tolerated (2, 3). RAL has been gradually replaced by next-generation INSTIs, such as dolutegravir (39), BIC, and cabotegravir (40). RAL is recommended as a second-line INSTI in the Guidelines for the Use of Antiretroviral Agents in Adults and Adolescents Living with HIV and the risk of drug-resistant HIV-1 (41). However, the drug has not yet been completely replaced, and RAL is currently prescribed to some patients in our hospital. In this study, we found that RAL containing a 1,3,4-oxadiazole ring was converted to the hydrolysate form, H-RAL at pH 1.0, which may occur in the stomach after meals.

Based on MW, LogP, CLogP, LogS, and TPSA scores, which are used to predict the oral bioavailability of drugs (42, 43), the fat solubility and cell membrane penetration of H-RAL are potentially lower than those of RAL. Despite these findings, some studies have shown that RAL has a favorable efficacy and safety profile when administered to treatment-naïve HIV-1 patients, with or without other class-resistant HIV (2, 3). In HIV treatment, combination antiretroviral therapy (ART) generally consists of three drugs that inhibit different stages of the HIV-1 replication cycle to prevent the emergence of drug-resistant HIV-1 strains (44), allowing patients with HIV-1 to suppress HIV-1 RNA levels (copies/mL) in the peripheral blood. Hence, other combination ART drugs may compensate for the occasional decrease in RAL efficacy. The medication package inserts state that RAL can be administered with or without meals. However, RAL should preferably not be administered after meals when the intragastric pH is low. Improved dosage forms such as controlled-release tablets or a combination with drug carriers such as CDs should be considered (45, 46).

Beta-CD, RAM-βCD, and HP-βCD have been used in various pharmaceutical applications (16, 17). Optimization of the method used to produce the inclusion complex (47) may increase the amount of RAL that is encapsulated within CDs, resulting in greater protection against conversion to H-RAL. In addition, encapsulation of drugs in modified CDs can also result in sustained release, leading to improved pharmacokinetics and more stable and long-term drug concentrations in the body (19, 48, 49). Actually, formulations of HP-βCD with antifungal drugs, such as itraconazole and posaconazole, have shown improved pharmacokinetics and are used in clinical applications (50, 51). The inclusion complexes of anti-HIV drugs and βCD derivatives were reported to improve pharmacokinetics and the anti-HIV efficacy of the drug after intravenous or oral administration in vitro and in vivo (52, 53).

Oral zibotentan did not lead to a statistically significant improvement in overall survival in patients with castration-resistant prostate cancer and bone metastases in a phase 3 trial (28). Zibotentan (ZD4054) containing a 1,3,4-oxadiazole ring was also predominantly converted to H-ZD4054 within a few hours at pH 1.0 (Fig. 2). Oral drugs with a 1,3,4-oxadiazole ring may be converted to hydrolysates with the cleaved 1,3,4-oxadiazole rings under highly acidic conditions in the stomach; thus, the loss of biochemical activity and bioavailability of 1,3,4-oxadiazole derivatives, after meals, should be considered.

Current ART allows HIV-1 patients to suppress the amount of HIV-RNA in the blood below the limit of detection (<20 copies/mL) and to recover immune system functions. Nevertheless, HIV-1 usually reactivates when ART is discontinued. HIV-1, a retrovirus, can remain latent as a provirus in reservoir cells or viral particles in deep tissues and are not targeted by current ART (54). The development of novel detection systems, such as positron emission tomography-computed tomography, capable of detecting such HIV reservoirs that escape into lymph nodes and deep tissues is expected (55). Enhanced ART, consisting of more potent antiretroviral drugs with or without effective devices such as CDs, might induce deeper HIV-1 suppression and contribute to reducing the HIV-1 reservoir size, potentially leading to an essential method for HIV cure. This approach could be also implemented in combination with available and novel treatment options (56–58). Encapsulation of RAL within CDs may lead to lower dosing, better medication adherence, and ultimately improved treatment outcomes in patients with HIV. However, further research is needed to investigate the efficacy and safety of CDs as drug-delivery systems for RAL, including potential adverse effects and drug interactions.

The reuse of potent previous-generation drugs with established efficacy and safety profiles may provide cost-effective treatment options for patients infected with HIV, including those in developing countries. Further research and development to optimize the use of anti-HIV drugs can lead to promising strategies to benefit patients with HIV worldwide.

Materials and methods

Cells, viruses, and viral quantification

MT-2 and MT-4 cells (Japanese Collection of Research Bioresources [JCRB] Cell Bank, Japan) were cultured in RPMI1640 medium (FUJIFILM Wako Pure Chemical Corporation, Japan) supplemented with 10% fetal bovine serum (FBS; Gibco, Thermo Fisher Scientific, USA), penicillin (P), and kanamycin (K). 293T cells obtained from the JCRB Cell Bank, and TZM-bl cells obtained from the NIH AIDS Research and Reference Reagent Program, were cultured in low-glucose dulbecco's modified eagle medium with

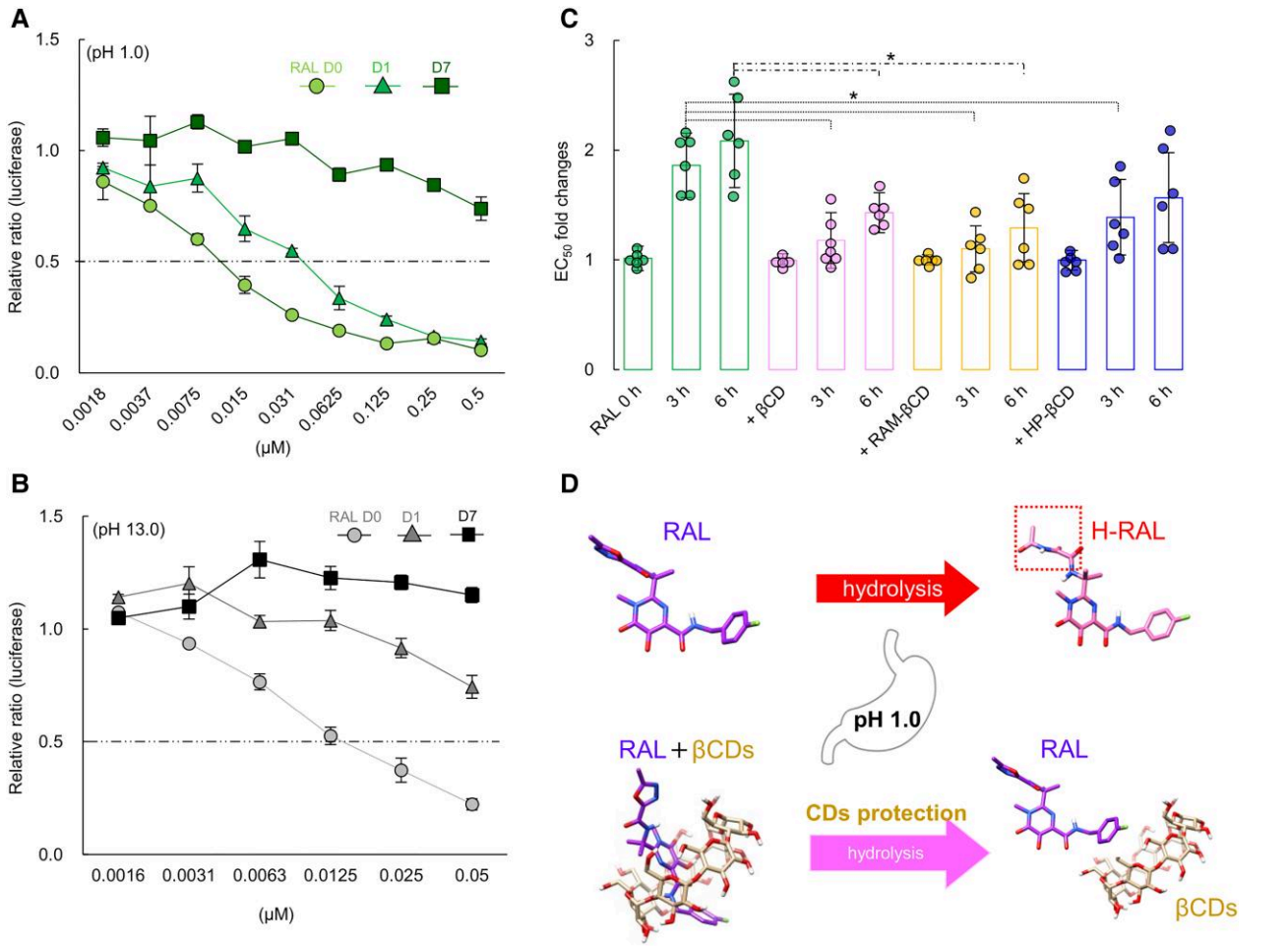

Fig. 6. Anti-HIV-1 activity of drugs post-treatment at pH 1.0 and CDs protection. The line graphs indicate the anti-HIV-1 infectivity at each concentration of RAL post-treatment at pH 1.0 A) and pH 13.0 B) by TZM-bl assay. C) The EC_{50}s fold changes at pH 1.0 for each 0, 3, and 6 h treatment of RAL alone shown in green, RAL plus βCD in pink, RAL plus RAM-βCD in yellow, and RAL plus HP-βCD in blue are shown as bar graphs with dot data. D) Schematic illustration showing that RAL was converted to H-RAL at pH 1.0 in the stomach, and the conversion was attenuated by βCDs. All assays were performed in duplicate, and error bars indicate ± SD from three independent experiments. Statistical significance between RAL and RAL plus βCDs at each incubation time was examined by Student's t test (*$P < 0.05$).

L-glutamine and phenol red (Fujifilm Wako) supplemented with 10% FBS, P, and K. The HIV-1 laboratory strain of HIV-1_{LAI} was propagated in MT-2 cells. HIV-$1_{NL4\text{-}3}$ and HIV-$1_{VSV\text{-}G\ dENV}$ were produced by transfection of the pNL4-3 or pCMV-VSV-G vector (Addgene, Watertown, MA, USA) plus pNL4-3 $_{dENV}$ into 293T cells, respectively (38). Virus samples were measured using an HIV-1 p24 enzyme-linked immunosorbent assay on Lumipulse G1200 (Fujirebio, Inc., Japan) and normalized to determine viral concentration.

pH adjustment and treatment

The pH 1.0 and 2.0 buffers were adjusted from 0.2 mol/L of KCl and HCl, respectively. The pH 3.0, 5.5, and 7.0 buffers were mixed with disodium hydrogen phosphate (Na_2HPO_4) and sodium dihydrogen phosphate dihydrate ($NaH_2PO_4\ 2H_2O$), and the pH 13.0 buffer containing KCl and NaOH were adjusted using the LAQUA twin-22B pH meter (HORIBA, Japan). Drugs tested were stored at −80 °C after treatment with the adjusted buffers for each time at 37 °C.

High-performance liquid chromatography

Drugs treated under various pH conditions were added to 50% (v/v) acetonitrile. After centrifugation at 2,500 rpm, the supernatant that included the drugs was examined using TSKgel ODS-100V, 100Z, or 120H columns (Tosoh Corp., Japan) at 1.0 mL/min in running buffer (50 mM phosphate buffer [pH 7.0] 50% acetonitrile). Samples (20 μL) were subjected to an Agilent Technologies 1220 Infinity LC system (Tosoh Corporation) and detected by measuring the optical density at 250–260 nm.

Surface plasmon resonance

SPR was examined using a Biacore X100 instrument (GE Healthcare) at room temperature (RT) multi-NH_2-CDs at 2 mM diluted in 25% dimethyl sulfoxide, DMSO, 10 mM disodium tetraborate [pH 8.5], and 1 M NaCl were immobilized on two flow cells of a CM5 sensor chip by direct amine coupling to over 1,000 response units. RAL diluted in HBS-EP buffer (10 mM HEPES, 150 mM NaCl, 3 mM EDTA, and 0.005% Tween 20) sterile was injected for 2 min at a flow rate of 30 μL/min followed by a 2 min dissociation step. Sensorgrams at each drug concentration were expressed using the Biacore X100 control software.

ESI mass spectrometry

Beta-CD, RAM-βCD, and HP-βCD were diluted to 1 μM and treated with either DMSO, RAL, or BIC, to a final concentration of 5 μM for

each compound in 5 mM ammonium acetate. Each sample solution was incubated at RT and introduced to the electrospray ionization quadrupole-time-of-flight (ESI-Q-TOF) mass spectrometer (impact II; Bruker Daltonics, Bremen, Germany) through an infusion pump at a flow rate of 3 μL/min. Samples were ionized in the positive ion mode with the following ion source parameters: dry heater: 200 °C, dry gas: 3.0 L/min, capillary voltage: 4,500 V, end plate offset: −400 V, and charging voltage: 2,000 V. MS scans were acquired at a spectra rate of 1 Hz in the mass range of 100–3,000 *m/z*. MWs were determined by deconvolution using DataAnalysis 4.4 (Bruker Daltonics).

LC-MS and LC-MS/MS (HR/MS) analyses

RAL samples at strong acidic or alkaline conditions were diluted with 0.5% acetonitrile in ultrapure water. The analysis was performed using a Q-TOF mass spectrometer equipped with a CaptiveSpray electrospray ionization platform in the positive mode (impact II) with LC (Ultimate 3000 HPLC; Thermo Fisher Scientific). One microliter of a prepared sample was injected and concentrated on an Acclaim PepMap 100 C18 trap column (Thermo Fisher Scientific) at a flow rate of 20 μL/min and separated on an Acclaim PepMap 100 C18 LC column (0.075 mm × 150 mm, 2 μm particle) (Thermo Fisher Scientific) at 30 °C column temperature; we used mobile phases A (0.1% formic acid in ultrapure water) and B (0.1% formic acid in acetonitrile) at a flow rate of 300 nL/min. For LC-MS/MS, the following gradient profile (*t* [min]/mobile phase B [%]) was used: 0/5, 5/5, 15/95, 19/95, 19.5/5, and 20/5. The data from the MS/MS experiments were acquired using the auto MS/MS acquisition mode. For the LC-MS analysis, an isocratic mode of 95% mobile phase B for 10 min was used. In both cases, the following ion source parameters were applied: dry heater: 150 °C, dry gas: 8.0 L/min, capillary voltage: 1,000 V, and end plate offset: −500 V. MS scans were acquired at a spectra rate of 1 Hz in the mass range of 50–1,000 *m/z*. QuantAnalysis Ver2.2.1 (Bruker Daltonics) was used to obtain MS and MS/MS spectra and identify the peak area of the chromatogram of *m/z* 445.16 as RAL or of *m/z* 463.17 as H-RAL. To determine the elemental compositions, mass accuracy of up to 5 ppm and isotopic distribution (mSigma) were used.

In silico simulation and docking model

The crystal structures of βCD (PDB accession number, 3CGT) were extracted from the RCSB Protein Data Bank (http://www.rcsb.org) and were used to produce the structures of βCD derivatives such as RAM-βCD and HP-βCD using SeeSAR v12.1 (BioSolveIT GmbH, Sankt Augustin, Germany). The crystal structures of PFV intasome (PDB accession numbers, 3L2V and 3OYA) and STLV-1 intasome (PDB accession numbers, 7OUG) from the RCSB Protein Data Bank were used for the docking simulation as the template model. All docking simulations were performed using SeeSAR v12.1. Molecular graphics and analyses were performed using UCSF Chimera (https://www.rbvi.ucsf.edu/chimera).

TZM-bl assay

The TZM-bl assay (38) was performed in 96-well black or white plates using a firefly luciferase reporter assay kit (PromoCell GmbH, Germany). Briefly, 50 μL of cells (10^5/mL) were seeded in the 96 wells and incubated for 24 h at 5% CO_2 and 37 °C. Diluted drugs mixed with viruses (25 ng/mL) plus diethyl aminoethyl-dextran (25 μg/mL) at final concentration were added to the cells (total final volume: 200 μL). After 48 h incubation, the supernatant medium switched to lysis buffer was shaken for 15 min, and D-luciferin was added to each well. Luciferase intensity was measured using a FLUOstar Omega instrument (BMG Labtech GmbH, Germany).

Drug susceptibility assay

The susceptibility of HIV-1_{LAI} (EC_{50}) and 50% cytotoxic concentration (CC_{50}) values to RAL, post-treated RAL at various pH conditions and control drugs were determined as previously reported (37).

Drugs

RAL, BIC, and DRV were purchased from Selleck Chemicals. Beta-CD, RAM-βCD, and HP-βCD were purchased from Tokyo Chemical Industry Co., Ltd (TCI), and the synthetic multi-NH_2-CDs were gifted by CyDing Company Limited.

Supplementary Material

Supplementary material is available at *PNAS Nexus* online.

Funding

This work was supported by the Japan Society for the Promotion of Science, KAKENHI grant number JP21K16324 (T.N.), and a grant from Takahashi Industrial and Economic Research Foundation, Takahashi grant number 131 (H.N.).

Author Contributions

T.N., T.H., and M.S. designed research; T.N., M.O., and N.T. performed research; N.T. and T.H. contributed new reagents or analytic tools; T.N., M.O., N.T., M.S., T.H., and H.N. analyzed data; N.T., T.H., M.S., J.Y., and H.N. edited the article; T.N., J.Y., and H.N. supervised personnel and the study; T.N. and N.T. wrote the article.

Data Availability

All data are included in the manuscript and/or supporting information.

References

1 Summa V, *et al.* 2008. Discovery of raltegravir, a potent, selective orally bioavailable HIV-integrase inhibitor for the treatment of HIV-AIDS infection. *J Med Chem*. 51:5843–5855.
2 Rockstroh JK, *et al.* 2013. Durable efficacy and safety of raltegravir versus efavirenz when combined with tenofovir/emtricitabine in treatment-naive HIV-1-infected patients: final 5-year results from STARTMRK. *J Acquir Immune Defic Syndr*. 63:77–85.
3 Eron JJ, *et al.* 2013. Efficacy and safety of raltegravir for treatment of HIV for 5 years in the BENCHMRK studies: final results of two randomised, placebo-controlled trials. *Lancet Infect Dis*. 13: 587–596.
4 Brainard DM, *et al.* 2011. Effect of low-, moderate-, and high-fat meals on raltegravir pharmacokinetics. *J Clin Pharmacol*. 51: 422–427.
5 Cattaneo D, *et al.* 2012. Inter- and intra-patient variability of raltegravir pharmacokinetics in HIV-1-infected subjects. *J Antimicrob Chemother*. 67:460–464.
6 Kiser JJ, *et al.* 2010. Effect of antacids on the pharmacokinetics of raltegravir in human immunodeficiency virus-seronegative volunteers. *Antimicrob Agents Chemother*. 54:4999–5003.

7 Iwamoto M, *et al.* 2009. Effects of omeprazole on plasma levels of raltegravir. *Clin Infect Dis*. 48:489–492.
8 Moss DM, Siccardi M, Back DJ, Owen A. 2013. Predicting intestinal absorption of raltegravir using a population-based ADME simulation. *J Antimicrob Chemother*. 68:1627–1634.
9 Moss DM, *et al.* 2012. Divalent metals and pH alter raltegravir disposition in vitro. *Antimicrob Agents Chemother*. 56:3020–3026.
10 Patil GD, *et al.* 2012. Identification, synthesis, and strategy for minimization of potential impurities observed in raltegravir potassium drug substance. *Org Process Res Dev*. 16:1422–1429.
11 Crini G. 2014. Review: a history of cyclodextrins. *Chem Rev*. 114: 10940–10975.
12 Jansook P, Ogawa N, Loftsson T. 2018. Cyclodextrins: structure, physicochemical properties and pharmaceutical applications. *Int J Pharm*. 535:272–284.
13 Fernàndez MA, De Rossi RH, Cervelló E, Jaime C. 2001. Effect of β-cyclodextrin on the hydrolysis of trifluoroacetate esters. *J Org Chem*. 66:4399–4404.
14 Medicines Agency European, Committee for Human Medicinal Products (CHMP). 2017. Questions and answers on cyclodextrins used as excipients in medicinal products for human use end of consultation. 44:1–8. https://www.ema.europa.eu/en/documents/scientific-guideline/questions-andanswers-cyclodextrins-used-excipients-medicinal-products-human-use_en.pdf.
15 Loftsson T, Masson M. 2001. Cyclodextrins in topical drug formulations: theory and practice. *Int J Pharm*. 225:15–30.
16 Loftsson T, Brewster ME. 2010. Pharmaceutical applications of cyclodextrins: basic science and product development. *J Pharm Pharmacol*. 62:1607–1621.
17 Loftsson T, Moya-Ortega MD, Alvarez-Lorenzo C, Concheiro A. 2016. Pharmacokinetics of cyclodextrins and drugs after oral and parenteral administration of drug/cyclodextrin complexes. *J Pharm Pharmacol*. 68:544–555.
18 Braga SS. 2019. Cyclodextrins: emerging medicines of the new millennium. *Biomolecules*. 9:801.
19 Hirayama F, Uekama K. 1999. Cyclodextrin-based controlled drug release system. *Adv Drug Deliv Rev*. 36:125–141.
20 Moriya T, *et al.* 1991. Potent inhibitory effect of a series of modified cyclodextrin sulfates on the replication of HIV-1 in vitro. *J Med Chem*. 34:2301–2304.
21 Graham DRM, Chertova E, Hilburn JM, Arthur LO, Hildreth JEK. 2003. Cholesterol depletion of human immunodeficiency virus type 1 and simian immunodeficiency virus with β-cyclodextrin inactivates and permeabilizes the virions: evidence for virion-associated lipid rafts. *J Virol*. 77:8237–8248.
22 Matassoli FL, *et al.* 2018. Hydroxypropyl-beta-cyclodextrin reduces inflammatory signaling from monocytes: possible implications for suppression of HIV chronic immune activation. *mSphere*. 3:1–13.
23 Tsiang M, *et al.* 2016. Antiviral activity of bictegravir (GS-9883), a novel potent HIV-1 integrase strand transfer inhibitor with an improved resistance profile. *Antimicrob Agents Chemother*. 60: 7086–7097.
24 Hayashi H, *et al.* 2014. Dimerization of HIV-1 protease occurs through two steps relating to the mechanism of protease dimerization inhibition by darunavir. *Proc Natl Acad Sci U S A*. 111: 12234–12239.
25 Alseekh S, *et al.* 2021. Mass spectrometry-based metabolomics: a guide for annotation, quantification and best reporting practices. *Nat Methods*. 18:747–756.
26 Siwach A, Verma PK. 2020. Therapeutic potential of oxadiazole or furadiazole containing compounds. *BMC Chem*. 14:1–40.
27 Bagnato A, Natali PG. 2004. Endothelin receptors as novel targets in tumor therapy. *J Transl Med*. 2:16.
28 Nelson JB, *et al.* 2012. Phase 3, randomized, placebo-controlled study of zibotentan (ZD4054) in patients with castration-resistant prostate cancer metastatic to bone. *Cancer*. 118:5709–5718.
29 Schmidt AK, Cottaz S, Driguez H, Schulz GE. 1998. Structure of cyclodextrin glycosyltransferase complexed with a derivative of its main product β-cyclodextrin. *Biochemistry*. 37:5909–5915.
30 Dotsikas Y, Loukas YL. 2003. Efficient determination and evaluation of model cyclodextrin complex binding constants by electrospray mass spectrometry. *J Am Soc Mass Spectrom*. 14: 1123–1129.
31 Pantaleão SQ, Fernandes PO, Gonçalves JE, Maltarollo VG, Honorio KM. 2022. Recent advances in the prediction of pharmacokinetics properties in drug design studies: a review. *ChemMedChem*. 17:e202100542.
32 Hare S, Gupta SS, Valkov E, Engelman A, Cherepanov P. 2010. Retroviral intasome assembly and inhibition of DNA strand transfer. *Nature*. 464:232–236.
33 Hare S, *et al.* 2010. Molecular mechanisms of retroviral integrase inhibition and the evolution of viral resistance. *Proc Natl Acad Sci U S A*. 107:20057–20062.
34 Krishnan L, *et al.* 2010. Structure-based modeling of the functional HIV-1 intasome and its inhibition. *Proc Natl Acad Sci U S A*. 107: 15910–15915.
35 Barski MS, *et al.* 2021. Structural basis for the inhibition of HTLV-1 integration inferred from cryo-EM deltaretroviral intasome structures. *Nat Commun*. 12:5927.
36 Meyer EA, Castellano RK, Diederich F. 2003. Interactions with aromatic rings in chemical and biological recognition. *Angew Chem Int Ed Engl*. 42:1210–1250.
37 Nakamura T, *et al.* 2020. A conformational escape reaction of HIV-1 against an allosteric integrase inhibitor. *J Virol*. 94: e00486-20.
38 Chia T, *et al.* 2021. A small molecule, ACAi-028, with anti-HIV-1 activity targets a novel hydrophobic pocket on HIV-1 capsid. *Antimicrob Agents Chemother*. 65:e0103921.
39 Boyd M. 2012. Dolutegravir—a promising antiretroviral in development. *Lancet Infect Dis*. 12:90–91.
40 Johns BA, *et al.* 2013. Carbamoyl pyridone HIV-1 integrase inhibitors 3. A diastereomeric approach to chiral nonracemic tricyclic ring systems and the discovery of dolutegravir (S/GSK1349572) and (S/GSK1265744). *J Med Chem*. 56:5901–5916.
41 Mbhele N, Chimukangara B, Gordon M. 2021. HIV-1 integrase strand transfer inhibitors: a review of current drugs, recent advances and drug resistance. *Int J Antimicrob Agents*. 57:106343.
42 Lipinski CA. 2004. Lead- and drug-like compounds: the rule-of-five revolution. *Drug Discov Today Technol*. 1:337–341.
43 Daina A, Michielin O, Zoete V. 2017. SwissADME: a free web tool to evaluate pharmacokinetics, drug-likeness and medicinal chemistry friendliness of small molecules. *Sci Rep*. 7:1–13.
44 Maenza J, Flexner C. 1998. Combination antiretroviral therapy for HIV infection. *Am Fam Physician*. 57:2789–2798.
45 Uekama K, Horiuchi Y, Irie T, Hirayama F. 1989. O-carboxymethyl-O-ethylcyclomalthoheptaose as a delayed-release-type drug carrier: improvement of the oral bioavailability of diltiazem in the dog. *Carbohydr Res*. 192:323–330.
46 Zheng D, Xia L, Ji H, Jin Z, Bai Y. 2020. A cyclodextrin-based controlled release system in the simulation of in vitro small intestine. *Molecules*. 25:1212.
47 Ghosh A, Biswas S, Ghosh T. 2011. Preparation and evaluation of silymarin β-cyclodextrin molecular inclusion complexes. *J Young Pharm*. 3:205–210.

48 Fattal E, Fay F. 2021. Nanomedicine-based delivery strategies for nucleic acid gene inhibitors in inflammatory diseases. *Adv Drug Deliv Rev*. 175:113809.
49 Hirotsu T, *et al.* 2017. Self-assembly PEGylation retaining activity (SPRA) technology via a host-guest interaction surpassing conventional PEGylation methods of proteins. *Mol Pharm*. 14:368–376.
50 Greer ND. 2007. Posaconazole (Noxafil): a new triazole antifungal agent. *Baylor Univ Med Cent Proc*. 20:188–196.
51 Mouton JW, *et al.* 2006. Pharmacokinetics of itraconazole and hydroxyitraconazole in healthy subjects after single and multiple doses of a novel formulation. *Antimicrob Agents Chemother*. 50: 4096–4102.
52 Buchanan CM, *et al.* 2008. Pharmacokinetics of saquinavir after intravenous and oral dosing of saquinavir: hydroxybutenyl-β-cyclodextrin formulations. *Biomacromolecules*. 9:305–313.
53 Adeoye O, *et al.* 2020. Pyromellitic dianhydride crosslinked soluble cyclodextrin polymers: synthesis, lopinavir release from sub-micron sized particles and anti-HIV-1 activity. *Int J Pharm*. 583:119356.
54 Chaillon A, *et al.* 2020. HIV persists throughout deep tissues with repopulation from multiple anatomical sources. *J Clin Invest*. 130: 1699–1712.
55 Beckford-Vera DR, *et al.* 2022. First-in-human immunoPET imaging of HIV-1 infection using 89Zr-labeled VRC01 broadly neutralizing antibody. *Nat Commun*. 13:1219.
56 Deeks SG, *et al.* 2021. Research priorities for an HIV cure: international AIDS Society Global Scientific Strategy 2021. *Nat Med*. 27:2085–2098.
57 Abner E, Jordan A. 2019. HIV "shock and kill" therapy: in need of revision. *Antiviral Res*. 166:19–34.
58 Fidler S, *et al.* 2020. Antiretroviral therapy alone versus antiretroviral therapy with a kick and kill approach, on measures of the HIV reservoir in participants with recent HIV infection (the RIVER trial): a phase 2, randomised trial. *Lancet*. 395:888–898.